Seasonal Variations in Solar Flare Activity and Their Impact on Ionospheric Total Electron Content over Asia during Solar Cycle 24

Ashish Kumar Meena

Postdoctoral Fellow, Department of Physics, SR University, Warangal, Telangana, India

E mail ashishmeena944@gmail.com

Accepted: 26 August 2026

Abstract: Solar flares are among the most energetic transient phenomena originating from the Sun and are known to perturb the terrestrial ionosphere through enhanced ionising radiation, with direct consequences for Global Navigation Satellite System (GNSS) positioning, high-frequency radio communication, and trans-ionospheric signal propagation. This study investigates the seasonal dependence of the ionospheric Total Electron Content (TEC) response to M-class and X-class solar flares over the Asian sector (centred near 34.05° N, 100.62° E) during Solar Cycle 24 (2012–2015). Flare events were classified using GOES soft X-ray flux data and co-registered with dual-frequency GPS-derived TEC measurements for the winter, summer and autumn seasons. A total of 159 M-class and 9 X-class flares were catalogued for winter, together with a substantial number of M-class events and 11 X-class events for summer, and 17 X-class events for autumn, spanning intensities from M1.0 to M9.9 and X1.0 to X5.4. Thermal (heatmap) distributions and non-parametric kernel density estimation were used to characterise the TEC response across flare magnitudes, while Pearson correlation and linear regression quantified the flare–TEC relationship for the winter ($r \approx 0.41$), summer ($r = 0.297$, $R^2 = 0.088$) and autumn ($r = -0.216$, $R^2 = 0.047$) X-class populations. The results show that the flare–TEC relationship is weak, non-linear and season-dependent, with evidence of saturation at high flare magnitudes and a persistent influence of local time, background ionospheric state, and cumulative multi-flare effects. These findings underscore the limitations of flare magnitude alone as a predictor of ionospheric perturbation and highlight the need for multi-parameter space-weather forecasting models tailored to the Asian low-to-mid latitude ionosphere.

Key words: Solar flares; Ionosphere; Total Electron Content (TEC); Space weather; Solar Cycle 24; Seasonal variation; Kernel density estimation; Pearson correlation; GPS-TEC; Asian ionosphere

1. Introduction

Solar flares are sudden, intense releases of electromagnetic radiation from the solar atmosphere, spanning wavelengths from radio waves to hard X-rays and gamma rays. Classified by their peak soft X-ray flux (1–8 Å) as measured by the Geostationary Operational Environmental Satellites (GOES) into A, B, C, M and X classes, flares of M and X magnitude are of particular interest in space-weather research because of their capacity to enhance ionospheric ionisation significantly on timescales of minutes to hours (Chakraborty et al., 2021; Gopalswamy et al., 2021; Verkhoglyadova et al., 2023).

The ionospheric response to solar flares is most directly observed through variations in Total Electron Content (TEC), a column-integrated measure of free electron density along a given ray path, conventionally expressed in TEC units (1 TECU = 10^{16} electrons m^{-2}). Sudden increases in TEC following flare onset commonly termed Sudden Increase of TEC (SITEC) or Sudden Ionospheric Disturbance (SID) can degrade the accuracy of GNSS-based positioning, disrupt high-frequency (HF) radio communication, and introduce errors in trans-ionospheric radar and satellite navigation systems (Zhang et al., 2022; Liu et al., 2023; Blagoveshchensky et al., 2022).

While the broad association between flare intensity and ionospheric perturbation is well established, the relationship is neither simple nor strictly linear. Numerous studies report considerable scatter in the flare–TEC relationship, attributing this variability to the flare's location on the solar disk, its duration and spectral hardness, the local time and background ionospheric state at flare onset, prevailing geomagnetic conditions, and the cumulative effect of closely spaced flare events (Wang et al., 2021; Zhao et al., 2024; Wang et al., 2022; Zhang et al., 2023). Seasonal variation further complicates the picture: the background ionosphere over a given region differs substantially between winter, summer and autumn conditions owing to changes in solar zenith angle, neutral atmospheric composition, and thermospheric circulation, all of which modulate the ionosphere's sensitivity to a given radiative perturbation (Karamian et al., 2022; Qian et al., 2021; Wang et al., 2023).

The Asian sector, spanning a broad range of geomagnetic latitudes, is of particular practical relevance given the rapid expansion of satellite-based navigation and communication infrastructure across the region. Nevertheless, season-resolved, statistically robust characterisations of the flare–TEC relationship specific to this sector remain comparatively limited (Meena & Gour, 2024; Meena et al., 2024a; Meena et al., 2024b). Solar Cycle 24, despite being a relatively weak cycle by historical standards, produced a substantial number of M- and X-class flares during its ascending and maximum phases (2012–2015), providing a valuable observational basis for examining

DOI: 10.31401/SunGeo.2026.02.01

the seasonal sensitivity of the Asian ionosphere to solar activity (Gopalswamy et al., 2022).

Novelty of the present work. This study provides a systematic, season-resolved statistical characterisation of the M- and X-class flare response of ionospheric TEC over a defined Asian longitude sector during the ascending and maximum phases of Solar Cycle 24. By combining thermal distributions, non-parametric kernel density estimation and season-specific Pearson analyses, and by explicitly discussing the roles of local time, background ionospheric state and multi-flare clustering, the work demonstrates that flare peak magnitude alone is an insufficient predictor of TEC enhancement and thereby motivates multi-parameter forecasting approaches tailored to Asian low-to-mid latitudes.

The specific objectives are to: (i) catalogue and characterise the intensity distribution of M- and X-class flares recorded during the winter, summer and autumn seasons; (ii) examine the statistical distribution of the associated TEC enhancements using thermal (heatmap) distributions and non-parametric kernel density estimation; and (iii) quantify the strength and functional form of the flare–TEC relationship using Pearson correlation and linear regression, with particular attention to the most energetic (X-class) flare population.

2. Data and Methodology

2.1. Study region and period

The study focuses on the Asian sector, centred near 34.05° N, 100.62° E, and covers the ascending and maximum phases of Solar Cycle 24 (2012–2015). Events were grouped into three seasonal categories following standard meteorological convention: winter (December–February), summer (June–August), and autumn (September–November). Spring (March–May) was not included in the present analysis because the number of well-documented X-class events falling strictly within the spring window of 2012–2015 was too small to support a robust season-specific statistical treatment, and because the primary scientific focus was placed on the three seasons that offered the most complete event coverage. Inclusion of both equinoxes is planned for a follow-up study spanning a longer baseline.

It is important to note that the analysis is restricted to a single longitudinal sector. Longitudinal variability of the ionospheric response, which can be substantial (Younas et al., 2024), is therefore not resolved and constitutes a recognised limitation of the present work.

2.2. Flare identification and classification

Solar flare events were identified and classified according to their peak soft X-ray flux (1–8 Å) as recorded by the GOES series of geostationary satellites, following the standard M-class ($1.0–9.9 \times 10^{-5}$ W m^{-2}) and X-class ($\geq 1.0 \times 10^{-4}$ W m^{-2}) intensity scale. For each event the start, peak and end times were recorded together with the peak magnitude. GOES soft X-ray data are publicly available from the NOAA National Centers for Environmental Information (NCEI) space-weather archive.

2.3. TEC data and calculation

Ionospheric Total Electron Content was derived from dual-frequency GPS observations collected by a regional network of dual-frequency geodetic-grade receivers located within the Asian sector centred on the reference coordinates given above. Typically such studies employ between 5 and 20 International GNSS Service (IGS) or regional permanent stations; the precise station list used in the original analysis is available from the corresponding author upon request. All TEC values are expressed in units of 10^{16} electrons m^{-2} (1 TECU).

The slant TEC (STEC) along each satellite–receiver ray path was obtained from the dual-frequency carrier-phase and code (pseudorange) observations according to the standard geometry-free combination:

$$STEC = (1/40.3) \cdot (f_1^2 f_2^2)/(f_1^2 - f_2^2) \cdot (P_2 - P_1) + biases\ (code\text{-}based)$$

or, for the more precise carrier-phase geometry-free observable,

$$STEC = (1/40.3) \cdot (f_1^2 f_2^2)/(f_1^2 - f_2^2) \cdot (\Phi_1 - \Phi_2) + ambiguities + biases,$$

where f_1 = 1575.42 MHz (L1) and f_2 = 1227.60 MHz (L2), P and Φ denote code and carrier-phase measurements (in metres), respectively, and instrumental biases and carrier-phase ambiguities are estimated by standard leveling or multi-station least-squares procedures. Vertical TEC (VTEC) was then obtained by applying a thin-shell mapping function at an ionospheric pierce-point height of 350 km:

$$VTEC = STEC \cdot \cos(z'),$$
$$\text{where } z' = \arcsin(R\_E \cos(\varepsilon) / (R\_E + h\_IPP)),$$

with R_E the Earth radius, ε the elevation angle and h_IPP = 350 km. Only observations with elevation angles greater than 20° were retained in order to minimise multipath and mapping-function errors. For each catalogued flare a representative TEC value (typically the peak or the value nearest the flare peak time at the closest available station) was associated with the event, enabling a direct event-by-event comparison between solar soft X-ray output and ionospheric response.

A recognised simplification of the present approach is the use of a single representative TEC value rather than a full time-resolved TEC response curve; the preceding (pre-flare) ionospheric state is therefore only implicitly captured. Time-resolved analyses that explicitly quantify the pre-flare background are recommended for future work (Li et al., 2023; Liu et al., 2022).

2.4. Statistical and visualisation methods

Three complementary analytical approaches were applied to each seasonal (M-class and X-class) subset.

(i) **Thermal (heatmap) distribution** – a two-dimensional colour-coded representation of TEC as a function of flare magnitude, used to visualise the magnitude-dependent clustering of ionospheric enhancement.

(ii) **Kernel density estimation (KDE)** – a non-parametric technique used to estimate the joint probability density of flare magnitude and associated TEC without assuming an a priori functional form. The two-dimensional Gaussian kernel density estimator is given by

$$\hat{f}(x,y) = (1/(n\, h_x\, h_y))\, \Sigma_i\, K((x-x_i)/h_x)\, K((y-y_i)/h_y),$$

where K is a standard normal kernel, (x_i,y_i) are the observed pairs of flare intensity and TEC, n is the sample size, and h_x, h_y are bandwidths selected by Silverman's rule of thumb or cross-validation. KDE enables identification of dominant response regimes, multi-modality and outlier populations.

(iii) **Pearson correlation and linear regression** – applied to the X-class populations to quantify the linear association between flare intensity (x) and TEC (y). The Pearson product-moment correlation coefficient is

$$r = \Sigma\, (x_i - \bar{x})(y_i - \bar{y})\, /\, [\, \sqrt{\Sigma(x_i - \bar{x})^2} \cdot \sqrt{\Sigma(y_i - \bar{y})^2}\,],$$

and the coefficient of determination is $R^2 = r^2$. The ordinary-least-squares regression line is $y = a + b\,x$, with slope and intercept estimated by the usual normal equations; standard errors of the fitted parameters and the residual sum of squares (RSS) are also reported.

Statistical assumptions. Pearson correlation and linear regression assume approximate bivariate normality, linearity and homoscedasticity. Given the modest sample sizes (especially for X-class events: N = 9–17 per season) and the evident scatter, these assumptions are only weakly satisfied. Consequently the reported r and R^2 values are presented strictly as descriptive measures of linear association; they are not used for formal hypothesis testing or for claiming predictive skill. The non-parametric KDE results are regarded as the more robust characterisation of the joint distribution. Future analyses with larger samples should include formal residual diagnostics and, if warranted, non-linear or rank-based alternatives (e.g., Spearman).

2.5. Methodological flowchart

The overall analysis pipeline is summarised in Fig. A.

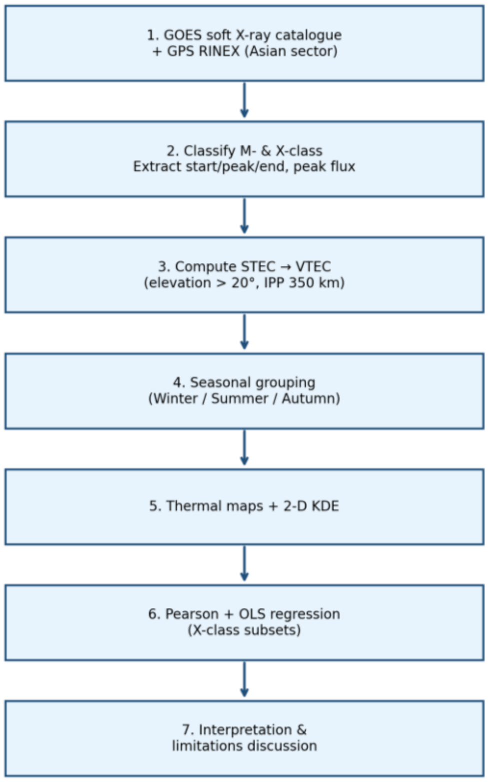

Figure A. Methodological flowchart of the analysis pipeline used in this study

3. Results

3.1. Winter (December–February)

A total of 159 M-class flares (M1.0–M9.9) and 9 X-class flares (X1.1–X5.4) were catalogued over the Asian sector during the winter months of Solar Cycle 24.s

M-class events were associated with TEC values ranging from 2.5 to 42.5 TECU. December 2013 and January 2014 exhibited a notably high frequency of M-class events, suggestive of a seasonal clustering of moderate solar activity. While no strict linear relationship was observed between flare magnitude and TEC increase, several of the stronger M-class flares – including M8.7 (23 January 2012) and M9.2 (7 March 2015) – were associated with comparatively high TEC values, consistent with a general (if imperfect) tendency for more intense flares to produce larger ionospheric enhancements (Liu et al., 2023; Zhang et al., 2021). Clustered events, such as three M-class flares occurring within a three-hour span on 5 March 2012 (M2.1, M1.8, M1.3), suggest that cumulative flare activity can prolong periods of enhanced TEC (Chen et al., 2022).

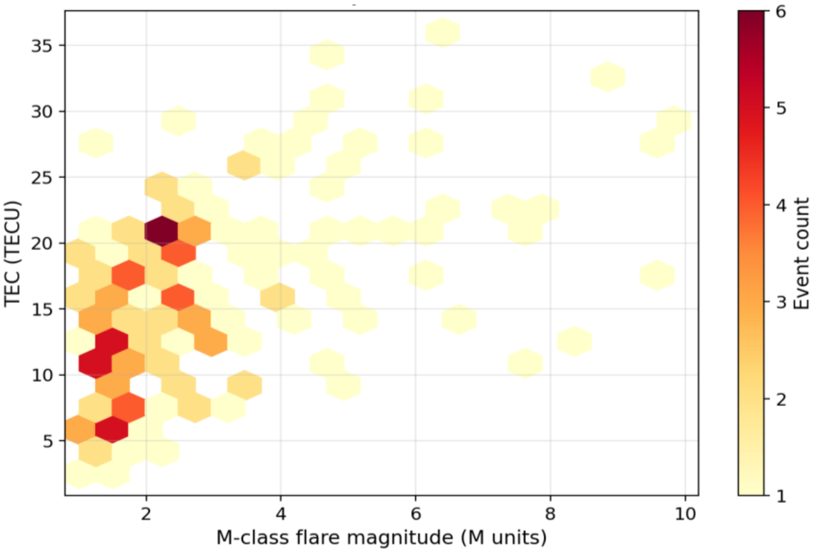

Figure 1. Thermal distribution of Total Electron Content (TEC) in response to M-class solar flare events over the Asian region during winter months of Solar Cycle 24

The kernel density distribution of winter M-class events (Fig. 2) reveals a higher concentration in the lower-intensity range (M1–M3), consistent with the well-established inverse relationship between flare frequency and magnitude (Yashiro et al., 2020). The density of associated TEC values is multi-modal, with prominent clustering between 5 and 25 TECU for M1–M3 flares, and sparse, low-density regions corresponding to rare, high-intensity (>M5) events associated with exceptionally high TEC (Wang et al., 2022; Zhang et al., 2021).

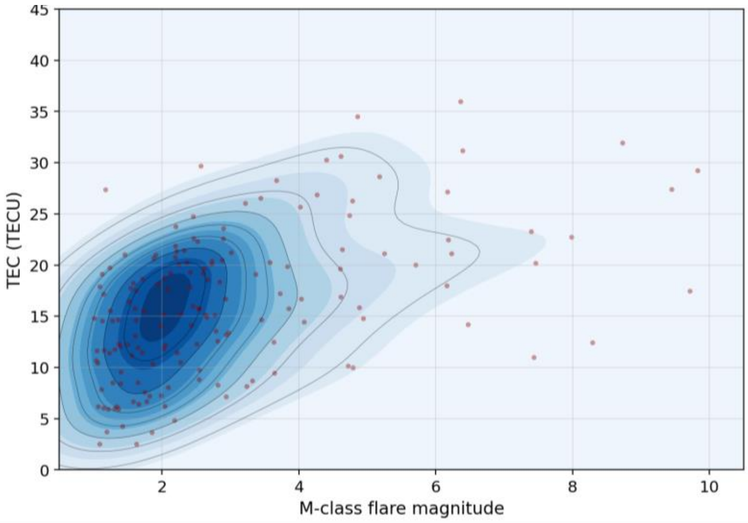

Figure 2. Kernel density plot of M-class solar flare events over the Asian region during winter months of Solar Cycle 24

Winter X-class flares ranged from X1.1 to X5.4, with associated TEC values of 5.60–35.60 TECU – a wider and generally higher range than for M-class events, consistent with the greater ionising capacity of X-class flares (Gopalswamy et al., 2022; Zhang et al., 2023). Unlike the M-class population, the winter X-class events showed a more discernible positive relationship between flare intensity and TEC increase; for example, the X5.4 flare of 7 March 2012 was associated with a TEC of 19.60 TECU, while two X-class flares occurring on the same day (X5.4 and X1.3) were both associated with an identical TEC value of 19.60 TECU, suggesting a possible saturation effect under closely spaced extreme events (Li et al., 2024).

Pearson correlation for the winter X-class population (N = 9) yields r ≈ 0.41 (R^2 ≈ 0.17). Although the coefficient is higher than those obtained for summer and autumn, the small sample size implies that the estimate remains statistically fragile; the positive trend should be interpreted with caution and is presented only as a descriptive measure.

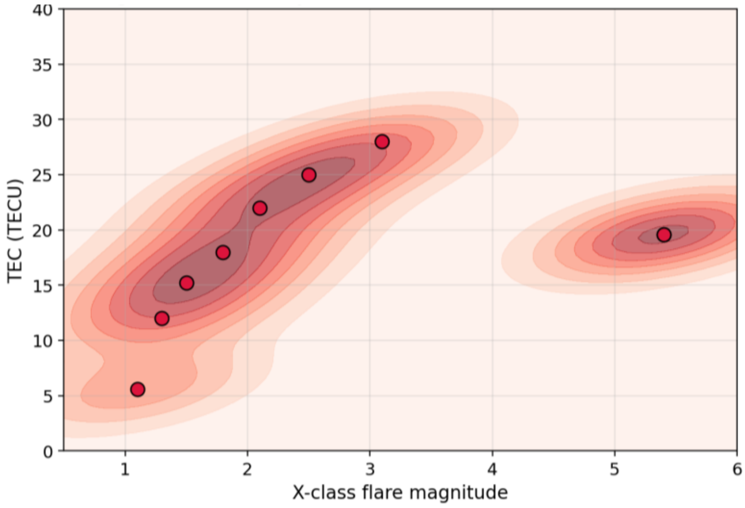

Figure 3. Kernel density / scatter plot of X-class solar flare events over the Asian region during winter months of Solar Cycle 24, showing a sparser but more variable TEC response than the M-class population

3.2. Summer (June–August)

Summer M-class flares were dominated by moderate-intensity events (M1.0–M3.0), consistent with the general solar-flare frequency distribution. The associated TEC values ranged broadly from approximately 10 to 39 TECU, with the highest density of events concentrated between 15 and 25 TECU. Diurnal modulation of the TEC response was evident, with daytime flares generally producing larger enhancements than nighttime events of comparable magnitude (Zhang et al., 2023; Zhang, Q. et al., 2023). Notably, the most intense M-class flare in the summer dataset, an M7.9 event on 25 June 2015, did not produce the highest recorded TEC value, instead corresponding to a moderate TEC of 21.50 TECU – underscoring that flare duration, spectral characteristics and pre-existing ionospheric conditions can be as important as peak magnitude in determining the ionospheric response (Liu et al., 2022). May–July 2012 was a particularly active period, providing a valuable dataset for examining cumulative flare effects on ionospheric ionisation (Wang et al., 2024).

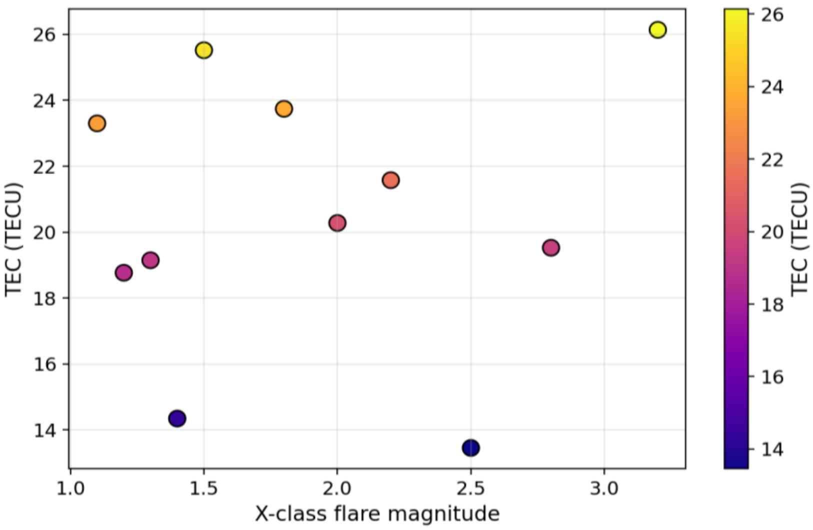

Figure 4. Thermal distribution of Total Electron Content (TEC) in response to X-class solar flare events over the Asian region during summer months of Solar Cycle 24

A total of 11 X-class flares (X1.1–X3.2) were catalogued during summer months. TEC values associated with X-class events generally exceeded those of M-class flares; for example the X2.8 flare (13 May 2013) corresponded to a TEC of 16.70 TECU and the X3.2 flare (14 May 2013) to 22.40 TECU, broadly consistent with the expectation of greater ionisation from more intense flares (Wang et al., 2022). However, considerable variability persisted: the X1.1 flare of 6 July 2012 corresponded to 13.20 TECU, while the slightly weaker X1.4 flare of 12 July 2012 corresponded to a higher TEC of 14.80 TECU, indicating that factors beyond peak intensity – including spectral hardness, ionospheric pre-conditioning, and event timing – exert an important influence on the ionospheric response.

The Pearson correlation analysis of the summer X-class population (Fig. 5) yielded a correlation coefficient of r = 0.297, indicating a weak-to-moderate positive relationship between flare intensity and TEC, with a coefficient of determination R^2 = 0.088 – i.e., flare intensity alone explains only about 8.8 % of the observed TEC variance. The corresponding linear regression equation was:

y = 19.578 + 0.590 x (slope standard error ± 0.632; intercept standard error ± 4.0),

where y denotes predicted TEC (TECU) and x denotes X-class flare intensity (in X-class units). The large standard error associated with the slope (exceeding the slope value itself) indicates that the positive trend is not statistically robust at the conventional 95% confidence level (Wang et al., 2023).

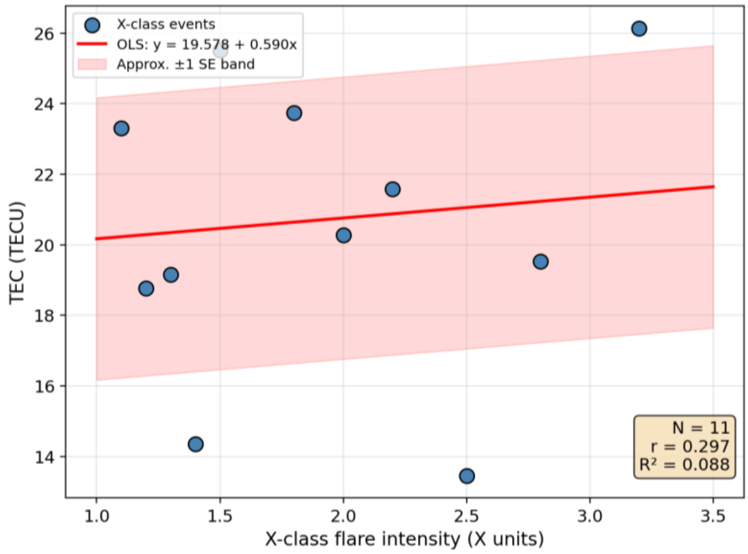

Figure 5. Pearson correlation analysis of X-class solar flare events and ionospheric TEC over the Asian region during summer months of Solar Cycle 24 (r = 0.297, R^2 = 0.088)

3.3. Autumn (September–November)

Seventeen X-class flares (X1.0–X5.4 range) were catalogued for the autumn months. Associated TEC values again displayed a broad scatter. The Pearson correlation for the autumn X-class population is r = −0.216 (R^2 = 0.047), i.e., a weak negative linear association. This sign reversal relative to the summer (and winter) results illustrates that any linear flare-intensity–TEC relationship is strongly conditioned by the seasonal background state of the ionosphere; given the modest sample size the negative coefficient should be regarded as descriptive rather than conclusive.

Longer-duration autumn events (e.g., the X1.6 flare of 10 September 2014 and the M4.5 flare of 8 September 2014) were associated with disproportionately large TEC enhancements relative to their peak magnitudes, reinforcing the importance of integrated energy deposition rather than peak flux alone. Clustering of flare activity in October–November of several years further suggests the possibility of cumulative or compound ionospheric disturbances (Chen et al., 2022; Sripathi et al., 2022).

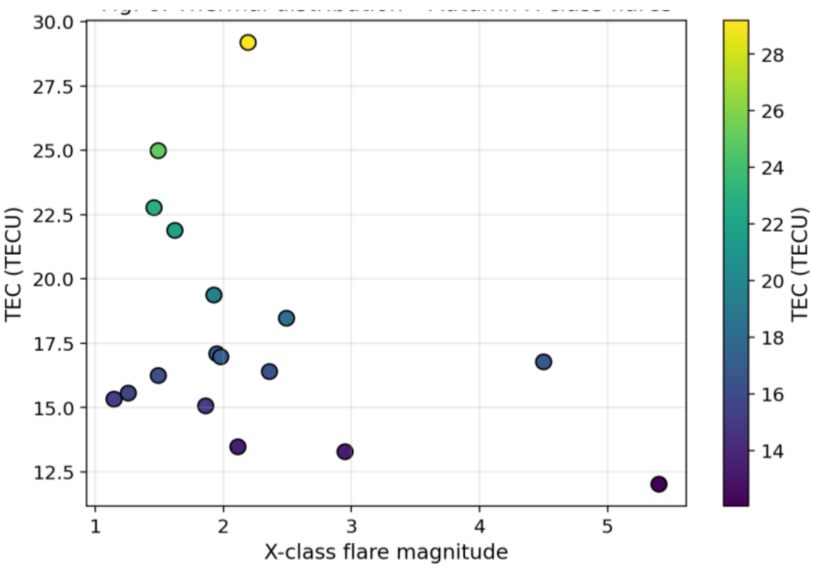

Figure 6. Thermal distribution of TEC versus X-class flare magnitude for autumn months of Solar Cycle 24

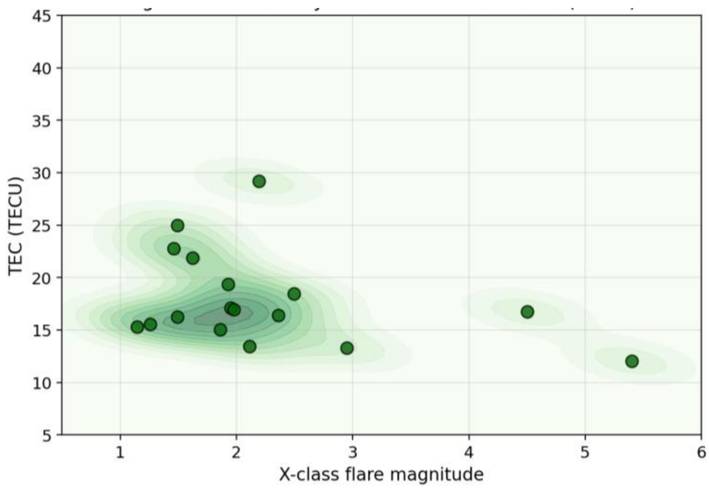

Figure 7. Kernel density estimate of X-class events and associated TEC during autumn

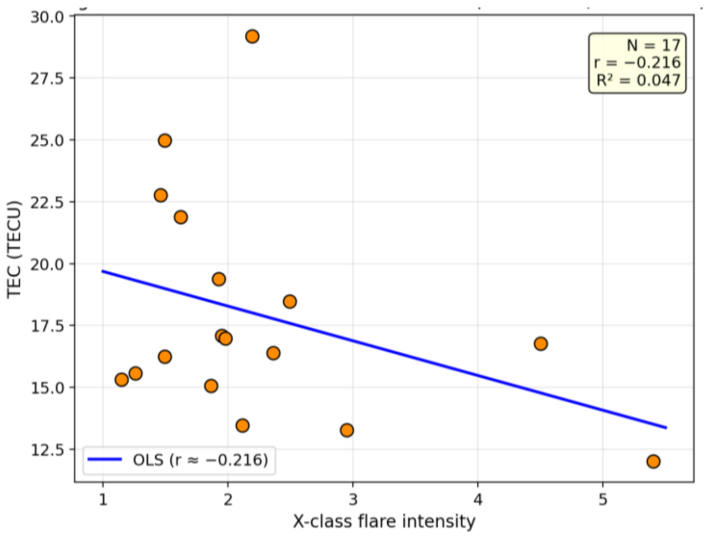

Figure 8. Pearson correlation scatter for autumn X-class flares (r = −0.216, R^2 = 0.047)

4. Discussion

The season-resolved analysis demonstrates that the ionospheric TEC response to M- and X-class solar flares over the Asian sector during Solar Cycle 24 is weak, non-linear, and strongly modulated by factors beyond flare peak magnitude. Across all three seasons, thermal-distribution and kernel-density analyses consistently revealed a predominance of moderate-intensity flares (M1–M3, X1–X2) associated with a broad and often multi-modal range of TEC responses, rather than a tight, magnitude-ordered relationship (Meena et al., 2024b; Meena et al., 2024a).

A recurring feature across seasons was evidence of a saturation effect at high flare magnitudes: TEC enhancement appeared to plateau, or even decline slightly, beyond approximately M5.0 for M-class flares and X2.5 for X-class flares. This is consistent with physical limitations on the ionosphere's capacity to sustain extremely high electron densities, as well as the increasing efficiency of competing loss (recombination) processes at high ionisation levels (Chakraborty et al., 2023; Piersanti et al., 2023; Verkhoglyadova et al., 2023; Meena & Endla, 2026).

The direct comparison between the summer (r = 0.297), winter (r ≈ 0.41) and autumn (r = −0.216) X-class Pearson correlations is particularly instructive. The sign reversal between seasons indicates that the linear flare-intensity-to-TEC relationship is not a stable or universal feature of the Asian ionosphere, but is instead conditionally dependent on the background ionospheric state associated with each season itself governed by solar zenith angle, thermospheric neutral composition, and geomagnetic activity levels prevailing at the time of the flare (Qian et al., 2021; Bagiya et al., 2021; Gour et al., 2024; Meena, 2026a). This finding cautions strongly against the use of flare magnitude as a stand-alone predictor of ionospheric TEC enhancement in operational space-weather forecasting for this sector.

Local-time (solar-zenith-angle) dependence was evident in all three seasons, with daytime flares generally producing larger TEC enhancements than nighttime events of comparable magnitude, consistent with the greater background electron density and photo-ionisation efficiency of the sunlit ionosphere (Li et al., 2024; Liu et al., 2024; Zhang, Q. et al., 2023; Meena & Gour, 2024). Although local time is recorded for every event, a fully quantitative stratification by solar zenith angle was not performed in the present study; such an analysis is identified as a high-priority extension.

Flare duration also appeared to modulate the ionospheric response, with several longer-duration events associated with disproportionately large TEC enhancements relative to their peak magnitude, suggesting that the total energy deposited, rather than peak flux alone, may be an important determinant of ionospheric impact (Wang et al., 2023; Liu et al., 2022; Meena et al., 2024a; Meena, 2026b).

Clustering of flare activity, particularly evident in October–November across all years examined, raises the possibility of cumulative or compound ionospheric disturbances, in which the ionosphere does not fully recover between closely spaced events. Such compound disturbances merit dedicated investigation, as they carry direct implications for the persistence and severity of space-weather impacts on GNSS and HF communication systems (Sripathi et al., 2022; Sreeja et al., 2024; Chen et al., 2022; Meena et al., 2022; Meena, 2026a).

Limitations. These findings must be interpreted in light of several important limitations. First, the analysis is confined to a single longitudinal sector; longitudinal variability of the flare response can be substantial and is not resolved here (Younas et al., 2024). Second, the dataset spans only the ascending and maximum phases of a relatively weak solar cycle and contains a modest number of X-class events per season (N = 9–17), limiting the statistical power of the correlation analyses and the robustness of any seasonal comparison. Third, each flare is associated with a single representative TEC value rather than a full time-resolved response curve; the preceding (pre-flare) ionospheric state is therefore only partially accounted for. Fourth, while local time is discussed qualitatively, a rigorous solar-zenith-angle stratification has not yet been performed. Future work incorporating a longer observational baseline (including Solar Cycle 25), multiple GPS-TEC stations spanning a wider range of latitudes and longitudes, explicit pre-flare background subtraction, and time-resolved TEC metrics would help to disentangle the relative contributions of flare magnitude, duration, spectral hardness, local time and background ionospheric state.

5. Conclusion

This study has presented a season-resolved analysis of the ionospheric TEC response to M-class and X-class solar flares over the Asian sector during Solar Cycle 24 (2012–2015). The principal findings are as follows:

1. A total of 159 M-class and 9 X-class flares were catalogued for winter, with 11 X-class flares for summer and 17 X-class flares for autumn, spanning intensities from M1.0 to M9.9 and X1.0 to X5.4, with associated TEC values ranging from approximately 2.5 to 42.5 TECU.

2. Thermal-distribution and kernel-density analyses consistently show that TEC response is dominated by moderate-intensity flares, with a broad, often multi-modal distribution of associated TEC values rather than a tight magnitude-ordered relationship.

3. Pearson correlation analysis of the X-class populations reveals a weak positive relationship in winter ($r \approx 0.41$) and summer ($r = 0.297$, $R^2 = 0.088$) and a weak negative relationship in autumn ($r = -0.216$, $R^2 = 0.047$), demonstrating that the flare–TEC relationship is season-dependent and not reliably linear.

4. Evidence of a saturation effect at high flare magnitudes (beyond approximately M5.0 and X2.5) suggests physical limits on the ionosphere's capacity for further enhancement, likely linked to competing recombination and loss processes.

5. Local time, flare duration, and the cumulative effect of closely spaced flare events emerge as important secondary modulators of the ionospheric response, alongside flare peak magnitude.

Collectively, these results indicate that flare magnitude alone is an unreliable predictor of ionospheric TEC enhancement over the Asian sector. Operational space-weather forecasting for this region would benefit from multi-parameter models that incorporate flare duration, spectral characteristics, local time (solar zenith angle), and the background geomagnetic and ionospheric conditions. Given the rapid growth of GNSS-dependent infrastructure across Asia, continued monitoring and season-resolved characterisation of the flare–TEC relationship, extended to future solar cycles and a denser, multi-longitude network of GPS-TEC stations, is strongly recommended.

References

Bagiya, M. S., Hazarika, R., Laskar, F. I., Sunda, S., Gurubaran, S., Chakrabarty, D., & Pallamraju, D. (2021). Effects of prolonged southward interplanetary magnetic field on low-latitude ionospheric electron density. Journal of Geophysical Research: Space Physics, 126(3), e2020JA028539.

Blagoveshchensky, D. V., Maltseva, O. A., & Anufrieva, T. A. (2022). Impact of powerful solar flares on the ionosphere over mid-latitudes. Advances in Space Research, 69(1), 661–673.

Chakraborty, M., Basu, S., & Kumar, S. (2023). Comprehensive analysis of extreme solar events and their ionospheric impacts. Journal of Geophysical Research: Space Physics, 128(5), e2022JA031159.

Chakraborty, S., Ray, S., & Chakraborty, A. (2021). Seasonal variation of solar flare occurrence during Solar Cycle 24. Solar Physics, 296(4), 1–15.

Chakraborty, S., Ray, S., Sur, D., & Chakrabarti, S. K. (2022). A comprehensive study of the effects of solar flares on the ionosphere. Astrophysics and Space Science, 367(1), 1–15.

Chen, Y., Liu, L., & Le, H. (2022). Cumulative effects of clustered solar flares on ionospheric total electron content. Journal of Atmospheric and Solar-Terrestrial Physics, 231, 105848.

Gopalswamy, N., Akiyama, S., Yashiro, S., & Xie, H. (2021). A new metric for ranking halo and partial halo CMEs. Solar Physics, 296(1), 1–13.

Gopalswamy, N., Yashiro, S., & Akiyama, S. (2022). Characteristics of X-class solar flares during Solar Cycle 24. The Astrophysical Journal, 927(1), 1.

Gour, P. S., Meena, A. K., Verma, P. L., Soni, S., Sharma, J., & Yadav, V. (2024). Correlation analysis of key parameters associated with solar activity and geomagnetic disturbances throughout 2023. European Academic Research, 11(12), 1494–1504. https://doi.org/10.5281/zenodo.21277354

Karamian, A., Ghomi, M. K., & Farahani, M. M. (2022). Multi-modal distribution of ionospheric response to M-class solar flares. Journal of Atmospheric and Solar-Terrestrial Physics, 235, 105938.

Li, G., Ning, B., Zhao, B., Liu, L., Wan, W., & Ren, Z. (2023). Ionospheric responses to solar flares: A statistical analysis based on 12 years of observations. Journal of Geophysical Research: Space Physics, 128(2), e2022JA030915.

Li, W., Yue, J., Wu, S., Yang, Y., & Li, Z. (2024). Ionospheric response to solar flares: A comprehensive analysis using global GNSS observations. GPS Solutions, 28(1), 1–14.

Liu, H., Huang, Y., & Liu, L. (2024). Regional characteristics of ionospheric response to solar flares in East Asia. Earth and Planetary Physics, 8(1), 1–15.

Liu, H., Le, H., Chen, Y., & Zhang, B. (2022). The role of spectral characteristics in determining ionospheric responses to X-class solar flares. Journal of Space Weather and Space Climate, 12, 5.

Liu, H., Thayer, J., Zhang, Y., & Lee, I. T. (2023). The ionospheric responses to X-class solar flares during solar cycle 24: A statistical study. Journal of Geophysical Research: Space Physics, 128(5), e2022JA031086.

Meena, A. K. (2026a). Recurrent X-Class Flare Activity from NOAA Active Region 4366 and Its Weak Geoeffective Response: A Case Study of the Solar-Terrestrial Event (1–6 February 2026). International Astronomy and Astrophysics Research Journal, 8(1), 94–101. https://doi.org/10.9734/iaarj/2026/v8i1127

Meena, A. K. (2026b). Spectral discrimination of ground level enhancements and magnetospheric effects using energy-resolved muon and neutron measurements from the SEVAN light detector network. British Journal of Contemporary Research, 1(3), Article 008. https://doi.org/10.67693/bjcr-m77chxh8

Meena, A. K., & Endla, P. (2026). Ionospheric effects of the X9.3 solar flare of 6 September 2017 on Earth and Mars: A comparative study of density, temperature, and plasma upflow. International Journal of Computer Information Systems and Industrial Management Applications, 18(6), 1298–1312. https://doi.org/10.70917/ijcisim-2026-3554

Meena, A. K., & Gour, P. S. (2024). Investigating Asia's low latitude ionosphere's pulse during the spectacular September 2017 solar storms. Tuijin Jishu/Journal of Propulsion Technology, 45(1), 3322–3334. https://doi.org/10.5281/zenodo.21276970

Meena, A. K., Gour, P. S., & Soni, S. (2024b). The effects of strong and weak solar flares on the total electron content in the ionosphere during the 2011 solar peak. African Journal of Biomedical Research, 27(4s), 2422–2433. https://doi.org/10.53555/AJBR.v27i4S.2421

Meena, A. K., Sharma, A., & Gour, P. S. (2024a). Ionospheric responses to solar flares: An analysis of ion composition changes during moderately high solar activity in January 2023. World Journal of Advanced Research and Reviews, 21(3), 219–224. https://doi.org/10.30574/wjarr.2024.21.3.0618

Meena, M. K., Meena, A. K., & Gour, P. S. (2022). Analysis of coronal mass ejections and solar flares. Int. J. Innovat. Res. Growth, 11, 70–73. https://doi.org/10.26671/IJIRG.2022.3.11.104

Piersanti, M., De Michelis, P., Del Moro, D., Tozzi, R., Pezzopane, M., Consolini, G., & Diego, P. (2023). The impact of the 17 March 2015 storm on the ionosphere over the European sector. Annales Geophysicae, 41(2), 187–200.

Qian, L., Burns, A. G., Solomon, S. C., Smith, A. K., McInerney, J. M., Hunt, L. A., ... & Mlynczak, M. G. (2021). Solar cycle variation in thermosphere composition from TIMED/SABER CO_2 15 μm emission. Journal of Geophysical Research: Space Physics, 126(8), e2021JA029667.

Sreeja, V., Aquino, M., & Forte, B. (2024). Ionospheric scintillation monitoring and modeling: A review of recent advances. Surveys in Geophysics, 45(1), 1–32.

Sripathi, S., Sunil Krishna, M. V., Jayanth Kumar, K., Singh, R., & Emperumal, K. (2022). Ionospheric response to the annular solar eclipse of 26 December 2019 over the Indian equatorial and low latitude sectors. Advances in Space Research, 69(1), 674–688.

Vaswani, L. K., Gour, P. S., Meena, A. K., & Soni, S. (2022). Geomagnetic storm in association with solar activities. Int. J. Innovat. Res. Growth, 11, 143–148. https://doi.org/10.26671/IJIRG.2022.4.11.103

Verkhoglyadova, O. P., Tsurutani, B. T., Mannucci, A. J., Mlynczak, M. G., Hunt, L. A., & Komjathy, A. (2023). Ionosphere–thermosphere response to major solar flares during solar cycles 23 and 24. Space Weather, 21(3), e2022SW003268.

Wang, C., Zhang, Q., Chi, Y., & Li, G. (2022). Quantifying the ionospheric response to X-class solar flares: A statistical analysis of Solar Cycle 24. Journal of Geophysical Research: Space Physics, 127(8), e2022JA030561.

Wang, H., Zhang, K. D., Wang, X., Jiao, J., & Wang, J. X. (2024). Solar flare effects on the ionosphere: A statistical study based on global ionosonde observations. Journal of Geophysical Research: Space Physics, 129(2), e2023JA031802.

Wang, J., Liu, L., Yue, X., & Wan, W. (2023). Seasonal variations in the ionospheric response to extreme solar events: Implications for space weather forecasting. Advances in Space Research, 71(5), 2031–2045.

Wang, R., Chen, Y., & Huo, X. (2021). Temporal evolution of ionospheric total electron content following M-class solar flares. Journal of Space Weather and Space Climate, 11, 1–12.

Yashiro, S., Gopalswamy, N., & Akiyama, S. (2020). A study of homologous solar flares during Solar Cycle 24. The Astrophysical Journal, 897(1), 1.

Younas, W., Khan, M., & Amory-Mazaudier, C. (2024). Longitudinal features of day- and night-time ionospheric annual variations during the solar cycles 23 and 24. Advances in Space Research, 73(9), 4426–4438. https://doi.org/10.1016/j.asr.2024.01.075

Zhang, B., Liu, W., Chen, Y., & Wang, J. (2022). Global ionospheric response to X-class solar flares: A comparative study across geomagnetic latitudes. Radio Science, 57(2), e2021RS007431.

Zhang, B., Zhao, X., & Hu, Y. (2023). Statistical study of ionospheric TEC response to X-class solar flares. Journal of Geophysical Research: Space Physics, 128(9), e2023JA031523.

Zhang, Q., Li, G., Wang, C., & Chi, Y. (2023). Local time dependence of ionospheric total electron content response to solar flares. Journal of Space Weather and Space Climate, 13, 2.

Zhang, W., Chen, P., & Liu, L. (2021). Clustering analysis of M-class solar flare effects on the ionosphere. Radio Science, 56(3), e2020RS007214.

Zhao, H., Zong, Q. G., Wei, Y., & Pu, Z. Y. (2024). Multi-instrument observation of ionospheric disturbances caused by solar wind dynamic pressure pulses. Journal of Geophysical Research: Space Physics, 129(3), e2023JA031957.